Exponential Escape Rate of Filamentary Incubation in Mott Spiking Neurons

Rodolfo Rocco, Javier del Valle, Henry Navarro, Pavel Salev, Ivan K. Schuller, and Marcelo Rozenberg

Phys. Rev. Applied **17**, 024028 — Published 9 February 2022

DOI: 10.1103/PhysRevApplied.17.024028

Exponential escape rate of filamentary incubation in Mott spiking neurons

Rodolfo Rocco,[1] Javier del Valle,[2,3] Henry Navarro,[2] Pavel Salev,[2] Ivan K. Schuller,[2] and Marcelo Rozenberg[1]

[1] *Université Paris-Saclay, CNRS Laboratoire de Physique des Solides, 91405, Orsay, France*
[2] *Department of Physics and Center for Advanced Nanoscience, University of California-San Diego, La Jolla, California 92093, USA*
[3] *Department of Quantum Matter Physics, University of Geneva, 24 Quai Ernest-Ansermet, 1211 Geneva, Switzerland*

(Dated: January 24, 2022)

Mott materials such as vanadium oxides, when subject to a strong applied voltage, present an inhomogeneous insulator-to-metal transition with formation of metallic filaments within the insulating bulk. This property is enabling the development of compact and power-efficient neuromorphic devices known as Mott neurons. However, the nature of the transition has not been fully understood yet, as it may be attributed to different effects, including Joule self-heating and hot carriers injection. Moreover, the experimental determination of the threshold voltage needed to induce the transition has proven to be challenging, as the transition becomes increasingly unpredictable when the threshold is approached. The physical understanding of these issues would not only deepen our understanding of Mott insulators, but would also be an important step toward the realization of neuromorphic devices based on such materials. In this work we use numerical simulations based on the Mott resistor network model to study the nature of the filament incubation and formation process. We show that both electronic and thermal effects, in the form of current density focusing and Joule self-heating respectively, contribute to the filamentary incubation and growth. Remarkably, we find that the percolation of the metallic filaments near the threshold is intrinsically stochastic, qualitatively similar to the familiar Arrhenius activated behavior and to the stochastic firing of biological neurons. More precisely, we characterize the filament percolation as a Poisson point process, which has the same probability distribution as mathematical models of neuronal firing with an exponential escape rate. Finally, we support the numerical simulation results by performing experiments in VO_2 that are in agreement with the exponential escape rate behavior. Thus, we establish a functionality of Mott insulators that opens a path towards implementing neuromorphic hardware with quantum materials.

I. INTRODUCTION

Large scale simulations of realistic neuronal models with high density of synaptic connections pose a computational challenge that has yet to be overcome by traditional von Neumann architectures [1]. Power efficiency and scalability are of particular concern, as the result of the different way in which the brain and computers are organized. More specifically, the separation of memory and processing elements that characterizes traditional computers has no equivalent in the brain, where neurons and synapses, the basic unit of computation and storage, are tightly integrated. One possible solution to this problem consists in the development of silicon neurons, i.e. neuromorphic circuits implemented with conventional semiconductor electronics, which mimic the functionality of biological spiking neurons [2]. These systems range from complex circuits that aim at faithfully reproducing mathematical neuron models [3, 4], to extremely simple ones counting very few components [5, 6].

However, the miniaturization and low energy consumption requirements are motivating a search for radically new devices based on quantum materials [7], such as Mott compounds, which exhibit metal-insulator transitions [8]. In fact, one recent example of these efforts is the Mott neuron [9], which is a realization of the leaky-integrate-fire neuronal model based on a chalcogenide Mott material [10]. Other notable examples of Mott materials which are currently being adopted are transition metal oxides, such as VO_2 [11, 12] and NbO_2 [13]. The potential for miniaturization, low power consumption and implementation of a wide variety of biological behaviours [14], make Mott neurons particularly promising. However, Mott neurons still pose great challenges in terms of reliable fabrication and, especially, electric control.

The spiking behavior of a Mott neuron device physically originates in the resistive collapse of the Mott insulator material upon the perturbation of the system by a strong electric field [15, 16]. The key insight is that applied voltage pulses, if frequent enough and strong enough, can induce the resistive collapse [17]. Thus, one may assimilate the pulses to the excitatory post-synaptic potentials of biological neurons, and the resistive collapse and ensuing current spike to the emission of an action potential [9].

Key to the neuromorphic functionality of Mott neurons is the *volatile* character of the resistive collapse. Namely, once the perturbation is terminated the collapsed resistance of the system spontaneously returns back to its original high insulating-state. This phenomenon is therefore qualitatively different from the better known and more common non-volatile resistive switching that enables the fabrication of synapses for neural networks and memory devices known as RRAM or memristors [7, 18, 19].

From the theoretical standpoint, the description of the

neuromorphic functionalities of Mott materials [20] requires the solution of many-body models of strongly correlated systems out-of-equilibrium and at strong electric fields, which remains a significant challenge [16, 21]. Nevertheless, valuable theoretical insights can be obtained from the study of mesoscopic-scale phenomenological models. One such model is the Mott Resistor Network (MRN) [11, 17, 22], which predicts the formation of a conductive filamentary structure within the stable insulator matrix as the triggering mechanism for the resistive collapse. This model prediction has recently been validated by direct observation of the filamentary incubation and growth in VO_2 [23]. An important aspect of the model is the assumption of the meta-stability of the metal phase, which is a characteristic of the metal-insulator transition in 3D Mott materials [8, 24]. This was recently put in evidence in a study of unexpected long-lasting memory in the relaxation dynamics of the resistive recovery of vanadium dioxide [11]. These effects were traced to the meta-stability of the metallic state, which causes a slow dissolution of the conductive filamentary structures [11, 22].

Different physical phenomena have been proposed to explain the filamentary formation process [25]. For instance, the resistive collapse may clearly be achieved by means of a purely thermal effect due to Joule self-heating. Indeed, applying a strong electric excitation beyond the ability of the device to dissipate the input power, would increase its temperature up to the critical insulator-metal transition temperature [16]. However, there is also another possibility that does not depend on a thermal effect. Mott insulators are not conventional insulators, but materials that would be metals if it were not for the correlation gap due to the strong Coulomb interactions [8]. This phenomenon occurs at exactly integer fillings of the conduction bands, so the Mott gap collapses upon electronic doping [20, 26]. Therefore, hot carrier injection at strong electric fields may drive the collapse of the Mott gap and the insulator state [15, 25, 27]. The relevance of this alternative route to the resistive switch was recently demonstrated in nanowire structures of vanadium oxides [28].

Besides the above mentioned debate on the filamentary formation process, other relevant questions on the physical mechanism remain. A prominent one is the issue of the voltage threshold, i.e. the minimal applied voltage required to induce the resistive collapse, which, rather surprisingly, is a challenge to precisely measure [11, 13]. Indeed, as the voltage threshold is approached the incubation time of the filament not only becomes very long, but it also becomes increasingly unpredictable. Understanding this feature is of key importance in order to build devices based on Mott materials whose operational limits can be reliably predicted.

In this paper we focus on this problem and clarify the nature of this filamentary resistive collapse. By numerical simulations of the MRN model, we gain insights of the coexistence and interplay of thermal and electronic effects in the filamentary formation. The former takes the form of inhomogeneous Joule self-heating and the latter of a current-density focusing effect resulting from the resistive change at the insulator-metal transition. A clarification is necessary at this point. By electronic effects we shall understand here not the many-body Mott collapse that we mentioned earlier, but a phenomenon that is driven by strong electric fields. As we shall see, approaching the point of the resistive collapse, the inhomogeneity of the electric field (due to geometry or possibly defects in a real device) may be dramatically enhanced due to the coupling of local self-heating and the insulator-metal transition phenomenon. This leads to the above mentioned current focusing effect and the ensuing conductive filament formation.

A significant result of our study is to show that the conductive filament formation in Mott materials can be understood as an activated phenomenon, qualitatively analogous to the familiar Arrhenius activation law, which is intrinsically stochastic. We validate our model simulation results by performing resistive switching experiments in vanadium dioxide devices. In addition, we also establish an interesting and rather unexpected connection between our findings and the behavior of biological neurons. Namely, we show that the statistical nature of the incubation time of the filaments in the resistive collapse closely mimics the intrinsic variability in the timings of spike-emission observed in biological neurons. More precisely, using the survivor function formalism, we show that the probability distribution of the resistive collapse follows the same form of the probability of spiking in theoretical neuronal models with an exponential escape rate [29–31].

II. RESULTS AND DISCUSSION

A. Mott Resistor Network Model

We focus on Mott materials that have a hysteretic first-order insulator-metal transition driven by temperature. Examples are VO_2, V_2O_3 and $NdNiO_3$, which have transitions at about $T_{IMT} = 340K$, $160K$ and $100K$, respectively [8]. When these materials are in their Mott insulating phase and subject to a strong applied voltage, in the range of kV/cm, they may suddenly undergo a sharp drop in their resistance after a certain time delay. The delay depends strongly on the applied voltage, and may span several orders of magnitude, from nsec to msec [11, 17, 23]. The nature of this resistive collapse has been explored in previous works, both experimentally and through Mott resistor network (MRN) model simulations [17, 22], and was found to be caused by the formation of low-resistivity filamentary domains within the material [9, 23, 32]. Since the MRN model is also at the basis of the simulations presented in this work, we shall describe it in this section. Further details can be found in the Methodology Section of the Appendix.

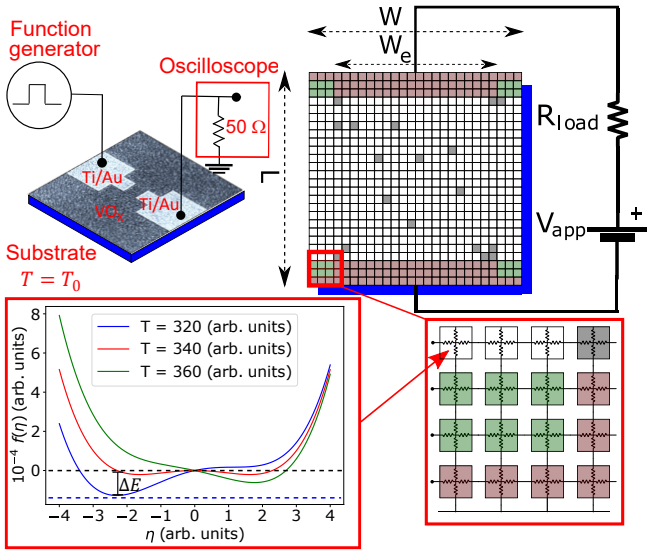

FIG. 1. Schematic diagram of the Mott Resistor Network model and the experimental setup [11]. Cells in red are ideal metal with zero resistivity and represent the electrodes. Cells in white and grey represent the thin film Mott material, which is assumed in thermal contact with a perfectly insulating substrate that is at $T_0 = 300$ arb. units (in blue). These cells can be either in the insulating (white, $\rho_{ins} = 3.5 \cdot 10^4$ arb. units) or metal (grey, $\rho_{met} = 10$ arb. units) states. Green cells are ideally insulating. The width of the sample is $W = 100$, that of the electrodes is $W_e = 42$ and the length of the sample is $L = 106$ cells. The gap between the electrodes is 100 cells long. Each cell is characterized by a Landau-type free energy that evolves with the temperature of the cell, as shown in the bottom inset figure. The two minima of the function correspond to either metal or insulating phase. The energy barrier ΔE of the insulating phase at three different temperatures is shown. A resistive termination (50Ω) after the function generator in the experimental setup was used when measuring the probability of transition (Fig.5) but not when measuring the incubation times (Fig.3).

The Mott resistor network (Fig.1) is a mesoscopic-scale phenomenological model where the device is divided into cells, each of which represents a nano-size region of the material. The size of the cells is assumed to be large enough so that they can be considered to be in one of two phases: either Mott insulator or correlated metal. In order to incorporate the first order character of the transition, we assume that the stability of the two phases depends on the local temperature via a free energy functional [22]. To give some order of magnitudes, the typical size of electrodes and the "gap" that separates them in experimental devices is 1-10μm, hence the size of of the cells in the model 10-100 nm [33]

When a voltage is applied across the network, currents start flowing through the resistors. Heat is locally generated in each cell in accordance with Joule's first law $P = I^2R$. The resistor network is assumed in thermal contact with a perfectly insulating substrate (depicted in blue in Fig.1). Each cell dissipates the produced heat by thermal conduction to its four neighbouring cells and to the substrate, that is assumed at a fixed temperature T_0. The thermal conductivity κ determines the magnitude of the heat transfer; for simplicity we assume the thermal conductivity to be the same for the dissipation to the substrate and to the nearest neighbours. Therefore, the temperature of each cell results from the action of two effects: a positive contribution, due to Joule heating, and a negative one, due to heat dissipation. The temperature equation can be written as:

$$\frac{dT_{ij}}{dt} = \frac{P_{ij}}{C} - \frac{\kappa}{C}\left(5T_{ij} - \sum_{kl}^{nn} T_{kl} - T_0\right) \qquad (1)$$

where ij and kl are the indexes of the cell, nn denotes nearest neighbours and C is its thermal capacity. In the limit of the thermal conductivity κ going to 0 and small applied voltages the film self-heats-up approximately homogeneously since the temperature gradients may be neglected. Then, the temperature change for the film as a whole can be written as:

$$\frac{dT}{dt} = \frac{I^2R(T)}{C} - \frac{K}{C}(T - T_0) \qquad (2)$$

where K is the thermal conductance of the interface, and C now denotes the heat capacity of the film. The temperature T_0 is assumed to be below the insulator to metal transition temperature T_{IMT}, thus, initially, all cells are in the insulating phase and have a high resistivity value ρ_{high}. When the cells undergo the transition to the correlated metal phase, their resistivity value changes to $\rho_{low} \ll \rho_{high}$. For simplicity, both resistivities are assumed to be independent of T, but the model can be easily generalized to include any temperature dependence [25]. One may think of the cells as qualitatively corresponding to the small crystalline grains of the actual Mott material film, which are of the order of tens of nanometers [33].

The transition of the cell is a thermally activated process that may occur even for temperatures lower than T_C, in accordance with the following transition rate:

$$\nu(T) = \nu_0 \exp\left(-\frac{\Delta E(T)}{T}\right) \qquad (3)$$

where T is the local temperature of the cell, $\Delta E(T)$ is the energy barrier of the cell free energy when it is in the insulating state, and ν_0 is the attempt rate [17]. The model can be simulated both in equilibrium and out of equilibrium, for small and large applied voltages, and also for arbitrary applied voltage protocols. In a simulation in equilibrium conditions, a minimal voltage, needed to probe the resistance, is applied. Then the temperature of the substrate is slowly raised. Under these conditions the system heats up in an approximately homogeneous

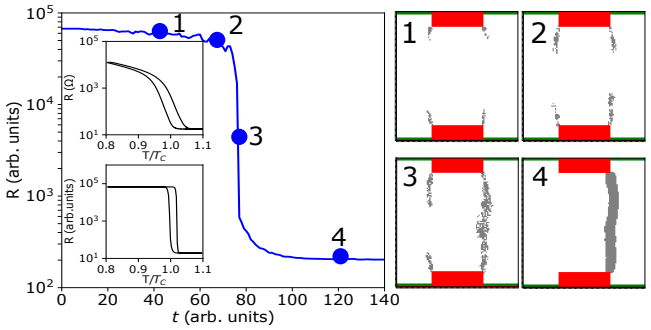

FIG. 2. The left panel shows the drop of the resistance of the simulated MRN when driven out of equilibrium by an applied voltage (blue curve, $V_{app} = 10^5$ arb. units, $K = 0.1$ arb. units). The top inset shows the experimental hysteresis curve for a VO_2 thin-film sample, the bottom one shows the curve produced by the model simulations in equilibrium conditions. The panels on the right show the resistivity map of the simulated system and the filamentary percolation of metallic cells. Similarly to Fig.1 the electrodes are in red, the cells in the insulating phase in white and the metallic cells in grey; green cells are perfectly insulating.

fashion. As the system crosses the critical T, the cells independently and randomly undergo local transitions and relaxations and no filamentary structure forms. As the temperature is raised beyond the transition temperature eventually all cells are in the metallic phase. After the transition, we gradually decrease the temperature of the substrate to the initial value, and from the computed $R(T)$ we obtain the hysteretic behaviour of the resistance. This is shown in the insets of Fig.2, where we compare the numerical results with experimental data on a VO_2 thin film sample.

When a strong voltage is applied, the system is driven out of equilibrium and the resistive transition is qualitatively different. The metallic phase takes a filamentary percolation form as is observed in the simulation data of Fig.2. We shall describe this phenomenon in further detail in the next sections.

B. Filamentary formation

A seminal discussion on the formation of inhomogeneous spatio-temporal structures of conduction was done by Ridley in the 60's [34]. As he pointed out, the origin of those dynamic instabilities could be traced to the presence of a negative differential resistance (NDR), as seen in the negative slope of the I-V characteristics of germanium with shallow impurity levels[34].

Mott materials do not have an evident intrinsic NDR. However, as mentioned in the introduction, two routes to NDR in thin-film devices are possible: self-heating and hot carrier injection. These two effects are *a priori* present in any thin-film devices and are reported in the phenomenon of *non-volatile* resistive switching in oxides such as TiO_2, HfO_2 among many others, where they lead to metallic filamentary structures [7, 18]. In those cases, the thermal runaway and high electric fields lead to electro-migration that changes the structure of the oxide thin-film, often creating massive number of defects such as oxygen vacancies. In contrast, Mott materials are qualitatively different since the thermal runaway and large fields are naturally quenched by the electronic Mott transition *without requiring any change of the film structure*. Hence, the volatile nature of the resistive switch.

The presence of an insulator-metal transition, with several orders of magnitude change in the resistivity, may also dramatically boost the magnitude of the NDR. Unfortunately, a rigorous theoretical description of this phenomenon is challenging. In fact, one is simulateneously dealing with a strongly correlated system away from equilibrium, inhomogeneous conduction states and large thermal and electric gradients. Hence, the need to recur to numerical simulations of the phenomenological model that we introduced before, in order to gain further insight on the origin and dynamics of the spatio-temporal instabilities, and to make contact with experiments.

Within the phenomenological model, the filamentary formation is a highly non-linear process that originates in a local thermal imbalance at large current densities. When a voltage is applied to the electrodes, a current begins to circulate through the Mott resistor network, and the cells start to generate heat, in accordance with Joule's law. At first, the rate at which the heat is generated is comparable to that at which it is dissipated to the substrate, which is in thermal contact with all cells and is kept at a fixed T_0. However, if the applied voltage is increased, the injected power eventually overcomes the ability of the substrate to absorb heat. In this situation, a local increase in the current (such as at the edges of the electrodes due to the point effect) leads to a local increase in temperature. Then, the probability that a hot cell becomes metallic also increases, since the transition is a thermally activated process. When a cell becomes metallic, its resistance decreases dramatically, since $\rho_{low} << \rho_{high}$. This draws more current from the neighboring cells to the metallic one, increasing its current density. This *current focusing* effect translates into further local heating, along with a dramatic increase of the transition probability of the neighboring cells that also heat up by Joule heating and by thermal conduction. Eventually, this process leads to the formation of conductive filaments that connect the electrodes. It is important to realize that for the resistive collapse to take place the device as a whole does not need to homogeneously reach the T_{IMT}. It is merely necessary that T_{IMT} is reached *locally* and that the NDR be strong enough (i.e. a significant ρ_{high}/ρ_{low} ratio [23]) to create the current focusing effect.

The previous qualitative discussion of the filamentary formation process is confirmed by the numerical simulations that we show in Fig.2. There we observe that, initially, the filaments emerge from the edges of the elec-

trodes and grow in approximately symmetric fashion, until they eventually connect. This is a manifestation of the familiar point-effect, namely, the enhancement of the electric fields near sharp angles. It is in these regions that the current density is initially stronger, even though the device cells are originally all identical and in the insulating state. The current gradients of geometrical origin act as seeds for the filamentary growth and have recently been directly imaged [23]. The growth of the filaments is correlated with the resistance of the device, as shown by the right hand side panel of Fig.2 and the respective points indicated along the collapse of the $R(t)$ in the main panel.

When the applied voltage is terminated, there is no more power input and the temperature of the cells relaxes back to $T_0 < T_{IMT}$, thus the device recovers the high resistance state. This *relaxation* of the filamentary structures has been studied in recent works [11, 22] and may be seen as the inverse of the filament incubation and growth that we consider here.

C. Incubation time: Purely thermal versus electro-thermal process

We would like now to systematically explore the process of filamentary formation. We shall see that several qualitatively different situations may be identified.

A useful quantity to characterize the formation of filaments is the delay time between the application of the external voltage and the observation of the resistive collapse, which we call the incubation time τ_{inc}. This quantity is directly accessible in experiments, which show that τ_{inc} depends strongly on the applied voltage, spanning several orders of magnitude. The lowest voltage that is required to observe a finite τ_{inc} is denoted the threshold voltage V_θ. As we shall discuss below, the determination of the threshold voltage may be more subtle than naively expected.

In the right panel of Fig.3 we show experimental data for the incubation times of VO_2 and V_2O_3 devices (see Fig.1 for the experimental setup). We notice that, for a relatively small variation of the applied voltage, τ_{inc} may change by orders of magnitude. Upon a closer look, we observe two qualitative features: one is a steep increase of τ_{inc} as the threshold voltage for resistive collapse, V_θ, is approached; the second is that the variability (i.e. the experimental error bars) of τ_{inc} also grows when decreasing the voltage. Moreover, in VO_2 the error bars are large and of the same order of magnitude as their respective mean τ_{inc}, and in the case of V_2O_3, they grow at an even higher rate approaching V_θ. This behavior indicates that the more the applied voltage approaches the threshold value, the more *unpredictable* the filamentary formation becomes, which questions the very notion of a well defined threshold voltage value.

To understand these experimental findings we turn our attention to the study of the MRN model. Since it has

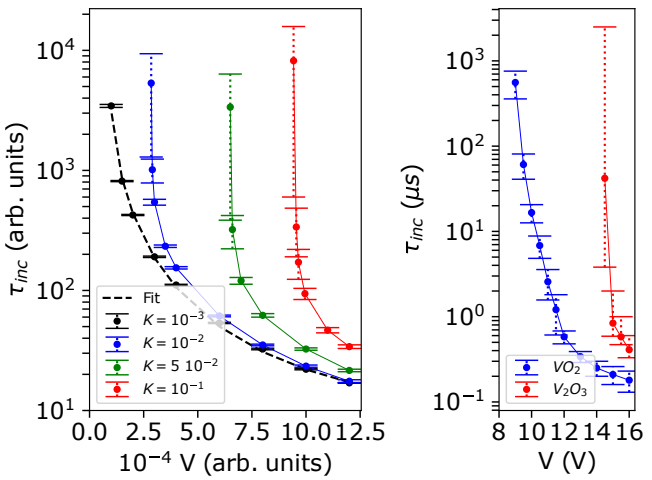

FIG. 3. In the left panel the incubation times produced by numerical simulations of the MRN model at different K values. The dashed black line is a fit using the expression Eq.6, while the other lines are simple guides to the eyes. In the right panel the incubation times measured for a VO_2 and a V_2O_3 device, in contact with substrates at $T = 334.9$K and 132K, respectively. The experimental data are the same as in [23].

several parameters, we need to choose a convenient way to explore the behavior of the resistive collapse. It has been experimentally observed that a relevant parameter is the ratio of the insulating and metallic resistivities ρ_{high}/ρ_{low} across the IMT [23]. However, for the systematic numerical model studying this parameter is not adequate. For instance, changing ρ_{low} alone produces little if any qualitative difference in the filamentary formation dynamics, since in the initial insulator state the power injection is determined by ρ_{high}. On the other hand, changing ρ_{high} alone is not possible, since one is forced to also modify the applied voltage to achieve the resistive collapse, which render the analysis more difficult. Thus, we find it most convenient to keep the values ρ_{high}, ρ_{low} and T_0 fixed and explore the different resistive collapse modes with the variation of a single parameter, the thermal conductivity K. In fact, it can be seen that K allows to capture two qualitatively different limits.

In the limit $K \to 0$ even a very low applied voltage produces self-heating as the cells do not dissipate the incoming power. The local self-heating is more intense at the edges of the electrodes, where the electric field and the current density are relatively larger, hence where the power is injected. Then it spreads out rather homogeneously in the bulk of the device. The self-heating continues at a rate set by the applied voltage, and since there is little dissipation, eventually the temperature of the bulk reaches T_{IMT} and the resistance collapses.

In contrast, in the limit of large K, a strong voltage *must* be applied to induce the resistive collapse, since the dissipation to the substrate brings thermal equilibrium at low injected power. Therefore, one expects stronger tem-

perature gradients and, consequently, stronger gradients of current density, which may lead to a less predictable resistive collapse. As we shall see below, in such a case, filamentary structures grow as in a sudden avalanche-like process, especially close to the threshold voltage.

The results of the simulations are shown in the left panel of Fig.3 where we plot the incubation time τ_{inc} as a function of the applied voltage for various values of the parameter K. We observe that several features of the experimental data shown in the right panel are present: Firstly, the range of τ_{inc} spans several decades for relatively small variations in the applied voltage. Secondly, there are two different regimes in $\tau_{inc}(V)$: The first one is at higher voltages, where $\tau_{inc}(V)$ shows a relatively weaker V-dependence and smaller error bars (that we thus refer to as "deterministic" regime). The second regime is at lower voltages, close to the threshold, which shows a steeper increase in τ_{inc} with V. Thirdly, this regime with relatively long incubation times also present large error bars, as in the experimental data. We thus refer to this regime as "stochastic", and is one of the main findings of the present study.

We shall argue now that the proper way of understanding the phenomenon of filament incubation in the latter regime is as a stochastic process due to a strong nonlinearity that couples a thermal imbalance and a current focusing effect, which results in a significant NDR.

A first insight comes from the observation that, in the limit of $K \to 0$, the transition becomes deterministic. This feature can be observed in Fig.3 where, in the limit of vanishing thermal conductivity, the variability of the incubation times remains small even close to the (low) threshold voltage. The deterministic nature of the resistive collapse in this case is further underlined by the fact that we can obtain an approximate analytic expression for $\tau_{inc}(V)$ by solving Eq.2 under the assumption of an homogeneous system and that the resistance of the sample stays constant and equal to R_{ins} before the transition. We can thus integrate Eq.2 to obtain the evolution of the temperature of the system as a function of time, then set T=T_{IMT} and invert the relation to get the thermal incubation time τ_{inc}^{th}:

$$\tau_{inc}^{th} = -\frac{C}{K}\ln\left(1 - \frac{KR_{ins}}{V^2}(T_{IMT} - T_0)\right) + \tau_0 \qquad (4)$$

where we used as a boundary condition $T(t=0) = T_0$ for the film's initial temperature. The small constant τ_0 is the physical minimal time that it may take the system to switch in the infinite V limit, which for the model is of the order of a few time-step.

We may define the thermal threshold voltage, V_θ, as the value of the applied voltage for which incubation times diverge:

$$V_\theta = \sqrt{KR_{ins}(T_{IMT} - T_0)} \qquad (5)$$

Thus, equation (4) can be rewritten as

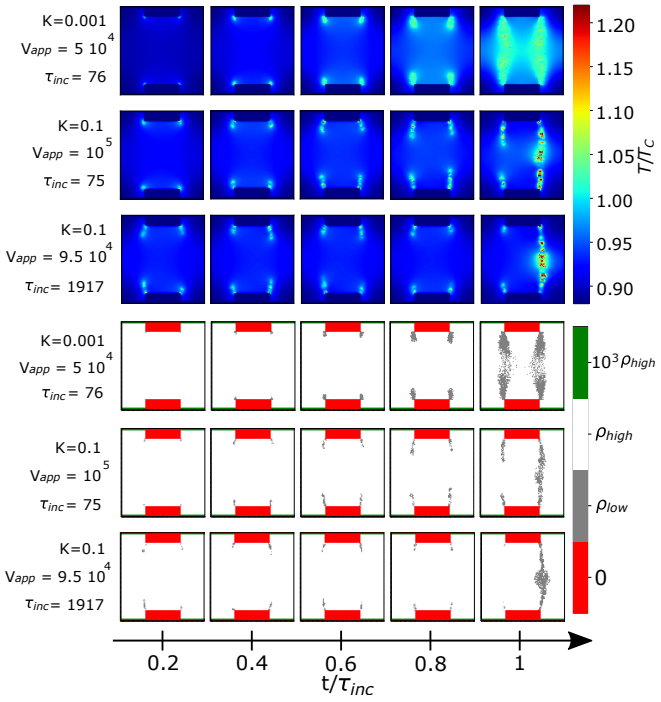

FIG. 4. Evolution of the temperature and resistivity maps of three different systems, one with small K in the thermal limit (top row, arb. units $\tau_{inc} = 76$ arb. units), and two with a large K in the electro-thermal limit (middle and bottom rows, with $\tau_{inc} = 75$ arb. units and $\tau_{inc} = 1917$ arb. units, respectively). The cases with high K differ in the value of the applied voltage: the bottom row is close to V_θ ($V_{app} = 9.5 \cdot 10^4$ arb.units), where the incubation times are highly stochastic, whereas the middle row is in the deterministic regime ($V_{app} = 10^5$ arb. units), which can be observed for high applied voltage in the incubation times curve of Fig.3. The panels capture snapshots of the state of the system as it progresses from the beginning of the filamentary formation up to the percolation, which corresponds to the resistive collapse of the system.

$$\tau_{inc}^{th}(V) = -\frac{C}{K}\ln\left(1 - \frac{V_\theta^2}{V^2}\right) + \tau_0 \qquad (6)$$

As shown in the left panel of Fig.3, this analytic expression provides an excellent fitting form for the numerical simulation data obtained at the smallest K. Thus, we may consider this behavior as the reference for a purely thermal resistive collapse due to self-heating alone.

We can now examine the dynamical evolution of the system as it evolves towards the resistive collapse at τ_{inc} by taking snapshots of the temperature and resistive maps of the MRN model. We find three different characteristic regimes (Fig.4). The panels of the top row depict the evolution when K is small, i.e. in the prototypical thermal case. We observe that the temperature gradients are relatively small, except at the edges of the electrodes. The heating in the central part of the system is gradual and homogeneous. The color code shows that

the temperature in the center reaches $T \approx T_{IMT}$ just before the resistive collapse (last panel).

The second row of panels of Fig.4 shows the temperature and resistance maps in the deterministic regime of large K. This occurs at voltages that are high compared to the threshold, where the error bars of τ_{inc} are relatively small (cf Fig.3). In this case we observe that, in contrast to the previous one, the central part of the system remains relatively cold, since the thermal conductivity to the substrate is better. From the maps we also observe the symmetrical and continuous growth of thin filamentary structures that originate at the sharp edges of the electrodes. The narrow metallic filaments result from the current focusing effect, since a large current density needs to develop to maintain those narrow structures locally above T_{IMT} when K is sizable. We note that the length of those filamentary structure grows rather linearly with time, until they span about half of the distance between electrodes. Then they percolate at the resistive collapse shown in the last panel. This linear in time progression is indicative of the deterministic behavior, that translates into the relatively small error bars in the respective incubation times (cf Fig.3).

In contrast to the previous cases, the third row of the panels of Fig.4 shows the stochastic regime. Here, K is relatively large and unchanged from the second row of panels, but the applied voltage is reduced to approach the threshold value. Consequently, the incubation time is now much longer. A significant difference, in sharp contrast with the previous case, is that the filaments do not grow but remain short stubs for most of the time. Eventually, one of them breaks the symmetry and a conductive filament suddenly grows and short-circuits the electrodes.This growth mode is not deterministic as in previous cases, where homogeneous self-heating (first case) or progressive linear growth of filaments (second case) was observed. The stochastic growth in the third case can be understood as a process with a very low probability of occurring which is nevertheless attempted during a very long time. In fact, the resistive collapse hinges on the insulator-to-metal transition rate of the cells. At low applied voltage this rate is relatively small, since the sample remains at a temperature beneath the T_{IMT} at all times, as most of the input power is efficiently dissipated to the substrate. Therefore, many attempts are needed to observe the percolation of the filament, which requires the simultaneous transition of several cells. Furthermore, since the attempts are independent of each other, the percolation event fulfils the conditions for a Poisson-like process, as we shall see in the next section.

In summary, the transition can have both a thermal and an electronic component. When the currents are not densely concentrated and the heat dissipation is poor, the sample heats up homogeneously and gradually to the transition temperature. In contrast, the electric component becomes significant when the thermal dissipation is better and a bigger electric power is injected. In this case, if the applied voltage is big compared to the threshold, the current focusing effect is strong and produces an inhomogeneous concentration of heat, which induces the continuous growth of filamentary structures. However, at applied voltages close to threshold, the generated heat is comparable to dissipation, leading to long incubation times that have a strong stochastic behavior.

Equipped with these insight, we can look back to the incubation time data of VO_2 and V_2O_3 samples (right panel of Fig.3). These are similar compounds, made on similar substrates and with similar K values [28].Nevertheless, we may note that V_2O_3 has a larger voltage threshold and larger resistivity ratio with larger error bars, which can be characterized as a resistive collapse with a stronger electric component. In contrast, VO_2 with smaller threshold voltage and smaller error bars is relatively closer to the thermal paradigm, consistently with previous experimental reports [28, 35, 36]. Nevertheless, the VO_2 data near the threshold still show a steep increase of incubation times and error bars that remain of the same order of τ_{inc}. This indicates that the electro-thermal effects also play a non-negligible role in the resistive collapse, as has been also reported in other previous experimental studies [37, 38]. Thus, our present work sheds light on the long lasting debate on the nature of the electrically triggered resistive transition in these materials, classifying VO_2 as a weak electro-thermal and V_2O_3 as a strong electro-thermal compound.

D. Stochastic filamentary incubation

We now turn to another main result of our work, where we shall demonstrate that vanadium oxide Mott neurons are capable of stochastic spike emission as observed in biological neurons. This is a remarkable feature that constitutes an unexpected *neuromorphic functionality* of these quantum materials.

Biological neurons emit spikes with an intrinsic stochastic component even under constant stimulation [29]. This feature is commonly described in mathematical models of neurons by an Arrhenius-like instantaneous probability of firing or exponential escape rate [29–31]:

$$f(u-\theta) = \frac{1}{\tau_s} \exp\left[(u-\theta)/\delta u\right] \tag{7}$$

where u is the neuron's membrane potential, θ is the membrane threshold, δu is the width of the membrane potential spike emission zone and τ_s is the mean time to spike emission at threshold [30]. From this mathematical expression, we can derive the probability $P(u,T)$ for the emission of a spike within a time window of duration T, when the potential is kept fixed at u. We shall show that the resulting probability also describes the probability of resistive collapse both in our Mott Resistor Network model and also in experiments done on a vanadium dioxide device.

The probability may be derived using the formalism of the survivor function [29]. Here we shall describe the main results (see Appendix for further details). The survivor function $S(T)$ is defined as the probability of *not* firing within a window of time T:

$$S(T) = 1 - P(u, T) \tag{8}$$

Using the instantaneous probability of firing $f(u-\theta)$ and keeping the potential u fixed, we may integrate the survivor function to get:

$$P(u, T) = 1 - \exp\left[-Tf(u-\theta)\right] \tag{9}$$

Inserting (7) and expanding the exponential, we finally get an approximate expression for the probability:

$$P(u, T) \approx 1 - \frac{1}{1 + \frac{T}{\tau_s}\exp[(u-\theta)/\delta u]}. \tag{10}$$

A connection with the MRN model and with experiments in Mott devices can be established by identifying the parameters of $P(u, T)$ as follows: The membrane potential u can be associated with the applied voltage V. The parameters δu and θ respectively become the fitting parameters δV and V_0. Finally, we take the microscopic time τ_s as equal to the time-step, which is the unit of time for the model simulations. Thus, we shall adopt as the fitting functional for the probability of filament formation within a time window T at applied voltage V the expression:

$$P(V, T) \approx 1 - \frac{1}{1 + T\exp[(V - V_0)/\delta V]}. \tag{11}$$

From this expression we may provide a proper definition of the firing voltage threshold, for a given arbitrary time window T. We call this quantity the stochastic threshold $V_S(T)$, which we define as the voltage value where the probability of incubating a filament is 1/2, i.e. $P(V_S, T) = 0.5$. Then, from Equation (11) we obtain:

$$V_S(T) = V_0 - \ln(T)\delta V \tag{12}$$

Since T is in units of time-step, it can't be smaller than $T = 1$ and thus the logarithm is always greater than zero. In Fig.(5), we show $P(V)$ for both the numerical simulations of the MRN model and experiments on a VO_2 device at room temperature. In this figure, $P(V)$ is the probability of observing the resistive collapse as a function of a constant applied voltage V, for different time windows T. The figure also shows how, in both cases, the probability expression derived above provides an excellent fit for the data. Interestingly, we also observe in the small panel of the figure that the behavior of $V_S(T)$

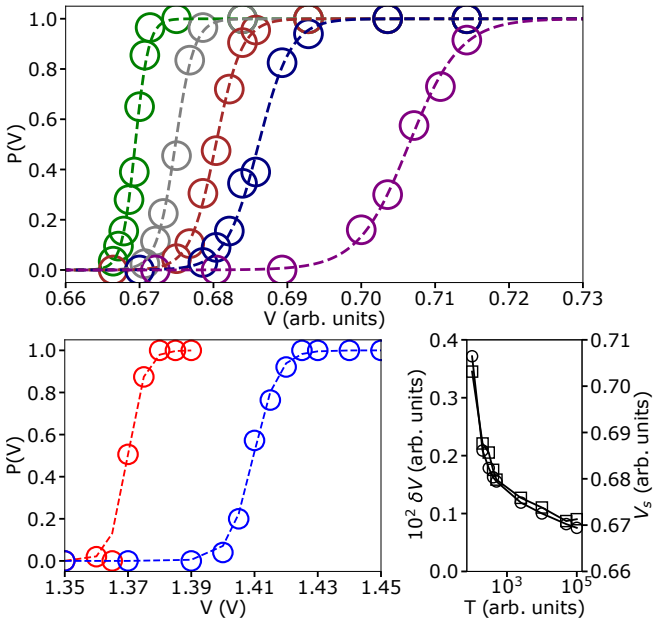

FIG. 5. The top panel shows the simulation results for the probability distribution of filament percolation for $K = 0.1$ arb. units and different values of the pulse width $T = 10^5$, $5{\cdot}10^4$, 2500, 400 and 100 arb. units from left to right. Voltage values are normalized by $V = 1.4 \cdot 10^5$ arb. units and for each point the total number of trials was 200. The fits were done using Eq. (11). The bottom left panel is the probability distribution obtained experimentally from a VO_2 sample, for two different pulse widths of $T = 10\ \mu s$ (red curve) and $T = 1\ \mu s$ (blue curve) and a substrate temperature of $T = 300$K. For the experimental details of the setup see Fig.1. The bottom right panel shows δV and V_S, the parameters of the fit to the simulation data in the top panel, evolve for different pulse widths. The fits to the experimental data were also done with Eq. (11) and the parameters are: $V_0(10\mu s) = 1.375$, $V_0(1\mu s) = 1.409$, $\delta V(10\mu s) = 0.002$ and $\delta V(1\mu s) = 0.003$. The size of the circles is comparable to the estimated binomial confidence intervals.

and δV closely track each other. We note that the latter is two orders of magnitude larger than the threshold voltage. This follows from the fact that δV characterizes the voltage transition range of a single cell, while V_S is the voltage applied between the electrodes. Since the distance between electrodes is L=100, the voltage drop on a single cell is of the order of V_S/L. We may further argue that since $V_S(T)$ characterizes the typical voltage value that induces a firing event in the time window T and δV the range of its stochastic behavior, then the underlying reason for the codependency is that the filamentary percolation, just like the firing event of spiking neurons, is a stochastic point process described by a Poisson distribution, which has the property of the mean being equal to its variance.

One final important observation is that our results also clarify the debated issue of the threshold voltage. In fact, in previous experimental work the problem of precisely determining the threshold voltage was already evident

[11]. This lack of precision was assumed to be caused by some source of experimental uncertainty. However, we now see that the dramatic enhancement of the error bars in the determination of the long incubation times at threshold is not an artifact but an intrinsic feature of the stochastic physical process of filamentary formation in Mott systems.

III. CONCLUSION

In this work we have shown that the percolation of metallic filaments, which triggers the electric-driven resistive collapse and the emission of a spike in Mott neurons [9], is a stochastic event. From the systematic study of the model we described in detail the highly non-linear electro-thermal process that drives the filamentary formation. More specifically, we have shown that while the filamentary formation is rather deterministic at high applied voltages, it becomes strongly stochastic as one approaches the voltage threshold. The stochastic behavior follows from the non-linearity of an electro-thermal process, in which the local insulator-metal transition produces a current focusing effect that leads to a negative differential resistance.

Two most common substrates for growing VO_2 thin films are Al_2O_3 and TiO_2. Thermal conductivity of Al_2O_3 is ≈ 25 W/(mK), which is much larger compared to the thermal conductivity of TiO_2 (≈ 5 W/(mK)). Therefore, according to our model, the switching of VO_2 grown on Al_2O_3 should display much more prominent stochastic behavior compared to the VO_2 prepared on TiO2. We note that with the recent progress of synthesis and transfer of nano-membranes [39] , high quality VO_2 films could be integrated with virtually any substrate. Using such nano-membrane approach, it is possible to test our model at extremes, for example, synthesizing VO_2 on a sulfur crystal (thermal conductivity ≈ 0.2 W/(mK) resulting in deterministic switching) or on diamond (thermal conductivity ≈ 2000 W/(mK) resulting in stochastic switching). From the practical point of view, the switching in VO_2 integrated with a pure silicon substrate, thermal conductivity ≈ 100 W/(mK), should be rather stochastic, while the switching in VO_2 on SiO_2, thermal conductivity ≈ 1 W/(mK), should be nearly deterministic.

Our Mott Resistor Network model simulations are validated by comparison to data from experiments on devices based on the Mott compounds VO_2 and V_2O_3. The analysis of the behaviour of the incubation times allowed us to characterize the resistive collapse in VO_2 and V_2O_3 as weak and strong electro-thermal, respectively, clarifying a longstanding debate.

Another significant result of the present work was to go beyond the qualitative description of the filamentary formation, to demonstrate that its stochastic behavior is characterized as a Poisson process. This is a remarkable finding, since spike emission in biological neurons can also be described as Poisson process. In fact, the probability distribution of the filament formation that we obtained and observed follows the same stochastic form as the spike emission in models of neurons with an exponential escape rate. Our results report an unexpected and exciting neuromorphic functionality of Mott materials, which adds to the potential of adopting these compounds as building blocks for future hardware in artificial intelligence systems.

IV. ACKNOWLEDGMENTS

We would like to thank C. Adda for useful discussions. We acknowledge support from the French ANR "MoMA" project ANR-19-CE30-0020. The experimental data in this work is part of the collaboration between UCSD and CNRS, in the Quantum Materials for Energy Efficient Neuromorphic Computing, an Energy Frontier Research Center funded by the US Department of Energy, Office of Science, Basic Energy Sciences under award DE-SC0019273.

[1] C. S. Thakur, J. L. Molin, G. Cauwenberghs, G. Indiveri, K. Kumar, N. Qiao, J. Schemmel, R. Wang, E. Chicca, J. Olson Hasler, *et al.*, Large-scale neuromorphic spiking array processors: A quest to mimic the brain, Frontiers In Neuroscience **12**, 891 (2018).

[2] G. Indiveri, B. Linares-Barranco, T. J. Hamilton, A. Van Schaik, R. Etienne-Cummings, T. Delbruck, S.-C. Liu, P. Dudek, P. Häfliger, S. Renaud, *et al.*, Neuromorphic silicon neuron circuits, Frontiers in Neuroscience **5**, 73 (2011).

[3] T. Yu and G. Cauwenberghs, Analog vlsi biophysical neurons and synapses with programmable membrane channel kinetics, IEEE Transactions on Biomedical circuits and Systems **4**, 139 (2010).

[4] S. Saighi, Y. Bornat, J. Tomas, G. Le Masson, and S. Renaud, A library of analog operators based on the hodgkin-huxley formalism for the design of tunable, real-time, silicon neurons, IEEE Transactions on Biomedical Circuits and Systems **5**, 3 (2010).

[5] M. Rozenberg, O. Schneegans, and P. Stoliar, An ultra-compact leaky-integrate-and-fire model for building spiking neural networks, Scientific Reports **9**, 1 (2019).

[6] P. Stoliar, O. Schneegans, and M. Rozenberg, Implementation of a minimal recurrent spiking neural network in a solid-state device, Physical Review Applied (in press).

[7] J. del Valle, J. G. Ramírez, M. J. Rozenberg, and I. K. Schuller, Challenges in materials and devices for resistive-switching-based neuromorphic computing, Journal of Applied Physics **124**, 211101 (2018).

[8] M. Imada, A. Fujimori, and Y. Tokura, Metal-insulator transitions, Reviews of Modern Physics **70**, 1039 (1998).

[9] P. Stoliar, J. Tranchant, B. Corraze, E. Janod, M.-P. Besland, F. Tesler, M. Rozenberg, and L. Cario, A leaky-integrate-and-fire neuron analog realized with a mott insulator, Advanced Functional Materials **27**, 1604740 (2017).

[10] C. Adda, B. Corraze, P. Stoliar, P. Diener, J. Tranchant, A. Filatre-Furcate, M. Fourmigué, D. Lorcy, M.-P. Besland, E. Janod, *et al.*, Mott insulators: A large class of materials for leaky integrate and fire (lif) artificial neuron, Journal of Applied Physics **124**, 152124 (2018).

[11] J. del Valle, P. Salev, F. Tesler, N. M. Vargas, Y. Kalcheim, P. Wang, J. Trastoy, M.-H. Lee, G. Kassabian, J. G. Ramírez, *et al.*, Subthreshold firing in mott nanodevices, Nature **569**, 388 (2019).

[12] J. del Valle, P. Salev, Y. Kalcheim, and I. K. Schuller, A caloritronics-based mott neuristor, Scientific Reports **10**, 1 (2020).

[13] S. Kumar, J. P. Strachan, and R. S. Williams, Chaotic dynamics in nanoscale nbo 2 mott memristors for analogue computing, Nature **548**, 318 (2017).

[14] P. Stoliar, O. Schneegans, and M. J. Rozenberg, Biologically relevant dynamical behaviors realized in an ultra-compact neuron model, Frontiers in Neuroscience **14**, 421 (2020).

[15] V. Guiot, L. Cario, E. Janod, B. Corraze, V. T. Phuoc, M. Rozenberg, P. Stoliar, T. Cren, and D. Roditchev, Avalanche breakdown in gata 4 se 8- x te x narrow-gap mott insulators, Nature Communications **4**, 1 (2013).

[16] J. Li, C. Aron, G. Kotliar, and J. E. Han, Microscopic theory of resistive switching in ordered insulators: electronic versus thermal mechanisms, Nano Letters **17**, 2994 (2017).

[17] P. Stoliar, L. Cario, E. Janod, B. Corraze, C. Guillot-Deudon, S. Salmon-Bourmand, V. Guiot, J. Tranchant, and M. Rozenberg, Universal electric-field-driven resistive transition in narrow-gap mott insulators, Advanced Materials **25**, 3222 (2013).

[18] J. J. Yang, D. B. Strukov, and D. R. Stewart, Memristive devices for computing, Nature Nanotechnology **8**, 13 (2013).

[19] E. Janod, J. Tranchant, B. Corraze, M. Querré, P. Stoliar, M. Rozenberg, T. Cren, D. Roditchev, V. T. Phuoc, M.-P. Besland, *et al.*, Resistive switching in mott insulators and correlated systems, Advanced Functional Materials **25**, 6287 (2015).

[20] A. Georges, G. Kotliar, W. Krauth, and M. J. Rozenberg, Dynamical mean-field theory of strongly correlated fermion systems and the limit of infinite dimensions, Reviews of Modern Physics **68**, 13 (1996).

[21] H. Aoki, N. Tsuji, M. Eckstein, M. Kollar, T. Oka, and P. Werner, Nonequilibrium dynamical mean-field theory and its applications, Reviews of Modern Physics **86**, 779 (2014).

[22] F. Tesler, C. Adda, J. Tranchant, B. Corraze, E. Janod, L. Cario, P. Stoliar, and M. Rozenberg, Relaxation of a spiking mott artificial neuron, Physical Review Applied **10**, 054001 (2018).

[23] J. Del Valle, N. M. Vargas, R. Rocco, P. Salev, Y. Kalcheim, P. N. Lapa, C. Adda, M.-H. Lee, P. Y. Wang, L. Fratino, *et al.*, Spatiotemporal characterization of the field-induced insulator-to-metal transition, Science (2021).

[24] A. Camjayi, C. Acha, R. Weht, M. Rodríguez, B. Corraze, E. Janod, L. Cario, and M. Rozenberg, First-order insulator-to-metal mott transition in the paramagnetic 3d system gata 4 se 8, Physical Review Letters **113**, 086404 (2014).

[25] P. Stoliar, M. Rozenberg, E. Janod, B. Corraze, J. Tranchant, and L. Cario, Nonthermal and purely electronic resistive switching in a mott memory, Physical Review B **90**, 045146 (2014).

[26] M. J. Rozenberg, Integer-filling metal-insulator transitions in the degenerate hubbard model, Physical Review B **55**, R4855 (1997).

[27] P. Diener, E. Janod, B. Corraze, M. Querré, C. Adda, M. Guilloux-Viry, S. Cordier, A. Camjayi, M. Rozenberg, M. Besland, *et al.*, How a dc electric field drives mott insulators out of equilibrium, Physical Review Letters **121**, 016601 (2018).

[28] Y. Kalcheim, A. Camjayi, J. del Valle, P. Salev, M. Rozenberg, and I. K. Schuller, Non-thermal resistive switching in mott insulator nanowires, Nature Communications **11**, 1 (2020).

[29] W. Gerstner, W. M. Kistler, R. Naud, and L. Paninski, *Neuronal dynamics: From single neurons to networks and models of cognition* (Cambridge University Press, 2014).

[30] R. Jolivet, A. Rauch, H.-R. Lüscher, and W. Gerstner, Predicting spike timing of neocortical pyramidal neurons by simple threshold models, Journal of Computational Neuroscience **21**, 35 (2006).

[31] H. E. Plesser and W. Gerstner, Noise in integrate-and-fire neurons: from stochastic input to escape rates, Neural Computation **12**, 367 (2000).

[32] H. Madan, M. Jerry, A. Pogrebnyakov, T. Mayer, and S. Datta, Quantitative mapping of phase coexistence in mott-peierls insulator during electronic and thermally driven phase transition, ACS nano **9**, 2009 (2015).

[33] J. del Valle, N. Ghazikhanian, Y. Kalcheim, J. Trastoy, M.-H. Lee, M. J. Rozenberg, and I. K. Schuller, Resistive asymmetry due to spatial confinement in first-order phase transitions, Phys. Rev. B **98**, 045123 (2018).

[34] B. Ridley, Specific negative resistance in solids, Proceedings of the Physical Society (1958-1967) **82**, 954 (1963).

[35] A. Zimmers, L. Aigouy, M. Mortier, A. Sharoni, S. Wang, K. West, J. Ramirez, and I. K. Schuller, Role of thermal heating on the voltage induced insulator-metal transition in vo 2, Physical Review Letters **110**, 056601 (2013).

[36] I. Valmianski, P. Wang, S. Wang, J. G. Ramirez, S. Guénon, and I. K. Schuller, Origin of the current-driven breakdown in vanadium oxides: thermal versus electronic, Physical Review B **98**, 195144 (2018).

[37] G. Gopalakrishnan, D. Ruzmetov, and S. Ramanathan, On the triggering mechanism for the metal–insulator transition in thin film vo 2 devices: electric field versus thermal effects, Journal of Materials Science **44**, 5345 (2009).

[38] G. Stefanovich, A. Pergament, and D. Stefanovich, Electrical switching and mott transition in vo2, Journal of Physics: Condensed Matter **12**, 8837 (2000).

[39] D. K. Lee, Y. Park, H. Sim, J. Park, Y. Kim, G.-Y. Kim, C.-B. Eom, S.-Y. Choi, and J. Son, Heterogeneous integration of single-crystalline rutile nanomembranes with steep phase transition on silicon substrates, Nature communications **12**, 1 (2021).

V. APPENDIX

A. The Mott Resistor Network model

The simulations used in this work are based on the Mott resistor network model, introduced in [17]. In this model the Mott material is represented by a mesh of resistors, as shown in Fig.1. The resistors are grouped into cells, each representing a small nanoscale region of the material. The cells in the top and bottom rows have zero resistivity (i.e. the resistance of the resistors within the cell is zero) and act as electrodes. When a voltage is applied across the mesh, currents flow through the resistors; knowing the initial value of the cells resistivity, and of the applied voltage, the currents can be computed by application of Kirchhoff law. When the currents flow through the resistors, these generate heat, due to the Joule effect, which can be computed as $P = I^2R$. The cells can dissipate heat to their nearest neighbours and to a thermal bath at temperature T_0. Therefore, the temperature increase of a cell will be given by the positive Joule heating contribution and the negative dissipation effect:

$$\frac{dT_{ij}}{dt} = \frac{P_{ij}}{C} - \frac{K}{C}\left(5T_{ij} - \sum_{kl}^{NN} T_{kl} - T_0\right) \tag{13}$$

where K is the thermal conductivity and C the thermal capacity; to avoid the proliferation of parameters, we make the non-essential assumption that the thermal conductivity is the same no matter whether the heat is dissipated to the thermal substrate or to any of the four nearest neighbours. In the case in which the temperature gradients can be neglected, we may consider the whole material instead of a single cell, and the equation is simply:

$$\frac{dT}{dt} = \frac{I^2R}{C} - \frac{K}{C}(T - T_0) \tag{14}$$

where I is the current that enters the mesh, R the resistance of the sample and T its temperature.

The cells can be in two states, insulating or metallic, to which correspond two resistivity values. These values are temperature independent, as evidenced by the comparison of the hysteresis produced by the simulations and the experimental hysteresis of a VO_2 sample, shown in the insets of the left panel of Fig.2. We use a Landau-type functional to describe the free energy [24] of the first order transition that occurs when a cell goes from one state to the other:

$$f(\eta) = h\eta + p\eta^2 + c\eta^4 \tag{15}$$

$$h = h_1\frac{T - T_{IMT}}{T_{IMT}} + h_2 \tag{16}$$

$$p = p_1\frac{T - T_{IMT}}{T_{IMT}} \tag{17}$$

Parameter	Value
h_1	$71.25 \cdot 10^3$
h_2	$7.5 \cdot 10^3$
p_1	$15.0 \cdot 10^3$
c	$3.0 \cdot 10^2$
T_{IMT}	380.0
T_0	300.0
ρ_{ins}	$3.5 \cdot 10^4$
ρ_{met}	10
R_L	$5 \cdot 10^3$
C	10
W	100
W_e	42
L	100
K	$[0.001, 0.1] \cdot C$

TABLE I. Values of the parameters used in the simulations.

where η is the order parameter and h_1, h_2, p_1, c and T_{IMT} are constants, T_{IMT} being the temperature of the insulator to metal transition. The values for the parameters used in the simulations are presented in Table I. The order parameter may be associated to observables, such as the lattice constants, which exhibit discontinuities at the transition [8]. The two local minima of the free energy correspond to the insulating and metallic states, and as the temperature of the cell increases, the energy barrier that separates them becomes smaller. The inset of Fig.1 shows the free energy landscape for three different temperature values.

The probability of transitioning from one state to the other is given by the law of Arrhenius:

$$p(T_{ij}) = \exp\left(-\frac{\Delta E(T_{ij})}{T_{ij}}\right) \tag{18}$$

where $\Delta E(T_{ij})$ is the energy barrier. Depending on the state the cell is in, its resistors will be assigned either a low resistance value, if metallic, or a high resistance, if insulating. The resistive collapse occurs when cells in the metallic state connect the two electrodes.

B. Probability of firing in a finite time interval and renewal statistics

Renewal theory describes the probability $P(t|\tilde{t})$ that an event, characterized by a stochastic intensity $\rho(t|\tilde{t})$ (also known as hazard function), will occur at time t given that the last occurrence was at time $\tilde{t}$. The firing of a neuron can be described as a renewal process if we assume that the probability of firing does not depend on the spike train but only on the time since the last spike. We notice that we cannot simply compute the probability that the

neuron should fire in a time interval T by integrating $\rho(t|\tilde{t})$ in said interval:

$$P(T) = \int_0^T \rho(t|0)dt \tag{19}$$

since $P(T)$ is not bounded by one. The proper approach to obtain this probability is to recur to the survivor function [29]. We define the survivor function $S(T)$ as the probability that the neuron will survive for a time T without firing:

$$S(T) = 1 - P(T) \tag{20}$$

We know for sure that, at time zero, the survivor function is equal to 1, and as time goes to infinity, since the probability of firing inevitably goes to 1, the survivor function goes to 0. Consequently, the survivor function decays proportionally to the rate at which the neuron attempts to fire, which defines the stochastic intensity:

$$\rho(t|0) = -\frac{dS(t)/dt}{S(t)} \tag{21}$$

Integration of this equation yields:

$$S(T) = \exp\left[-\int_0^T \rho(t|0)dt\right] \tag{22}$$

The survivor function can be put back into equation (20) to obtain the probability that the stochastic event will occur in a finite time interval. In our case the event is the firing of a noisy neuron, therefore the stochastic intensity takes the form of the instantaneous firing probability $f(u(t) - \theta)$:

$$P(T) = 1 - \exp\left[-\int_0^T f(u(t) - \theta)dt\right] = \tag{23}$$
$$= 1 - \frac{1}{\exp\left[\int_0^T f(u(t) - \theta)dt\right]}$$

If we assume that $u(t)$ stays constant in the interval T, which is the case if $u(t)$ represents the voltage applied to the Mott device before the resistive transition occurs, then the integral may be approximated as the product of the integrand times the interval, i.e., $T\ f(u - \theta)$

$$P(u, T) = 1 - \frac{1}{\exp\left[Tf(u - \theta)\right]} \tag{24}$$

To simplify this expression, we may expand the exponential to the first order since the argument is large outside the region of interest, i.e. $T \gg 0$ or $u \gg \theta$, where the probability approaches unity anyway. Thus, we get:

$$P(u, T) \approx 1 - \frac{1}{1 + Tf(u - \theta)} \tag{25}$$

and, finally, substituting the instantaneous firing probability $f(V - V_\theta) = \frac{1}{\tau_s}\exp[(u - \theta)/\delta u]$ in the equation yields the functional form that we used to fit the probability distribution of filament percolation:

$$P(V, T) \approx 1 - \frac{1}{1 + \frac{T}{\tau_s}\exp[(u - \theta)/\delta u]} \tag{26}$$